ELSEVIER

Solid State Ionics 110 (1998) 303–310

SOLID STATE IONICS

Transport properties of $SrCe_{0.95}Y_{0.05}O_{3-\delta}$ and its application for hydrogen separation

Jie Guan[a], Stephen E. Dorris[a], Uthamalingam Balachandran[a,*], Meilin Liu[b]

[a]*Energy Technology Division, Argonne National Laboratory, Argonne, IL 60439, USA*
[b]*School of Materials Science and Engineering, Georgia Institute of Technology, Atlanta, GA 30332, USA*

Received 5 March 1998; accepted 4 April 1998

Abstract

Transport properties of $SrCe_{0.95}Y_{0.05}O_{3-\delta}$ were studied by impedance spectroscopy and by measuring open-cell voltage (OCV) and gas permeation. Ionic transference numbers were determined by measuring the OCV of concentration cells and water vapor evolution of an O_2/H_2 fuel cell. We observed interfacial polarization on the basis of the *I–V* curves obtained by discharging a hydrogen concentration cell or an O_2/H_2 fuel cell. The observed high protonic conductivity (high proton and low oxide ion transference numbers) makes $SrCe_{0.95}Y_{0.05}O_{3-\delta}$ a potential material for hydrogen separation. From proton conductivity measurements, under a given hydrogen partial pressure difference of 4%/0.488%, the hydrogen permeation rate (of a dense membrane with 0.11 cm in thickness) was calculated to be ≈ 0.072 cm^3 (STP) cm^{-2} min^{-1} at 800°C, whereas the permeation rate calculated from short-circuit current measurements was ≈ 0.023 cm^3 (STP) cm^{-2} min^{-1} at 800°C. The difference between calculated and observed permeation rates is probably due to interfacial polarization.

Keywords: Fuel cell; Gas separation; Mixed conductor; Solid-state electrolyte; H_2 separation

1. Introduction

It is of great interest to use a mixed ionic–electronic conductor (MIEC) for gas separation because of its simplicity and cost-effectiveness [1,2]. A membrane of a mixed protonic–electronic conductor may be useful for H_2 separation if the electronic and protonic conductivities are well tailored.

With proper doping, perovskite-type oxides have shown high-temperature proton conductivity in hydrogen-containing atmospheres [3–5]. When compared with $SrCeO_3$-based materials, $BaCeO_3$-based materials have higher conductivity but also show substantial oxide ion conduction in the presence of oxygen gas or water vapor. The oxide ion conduction, however, does not make any useful contributions in hydrogen separation applications. As Iwahara et al. [6], Taniguchi et al. [7], and Bonanos et al. [8] have shown, proton conduction is favored at lower temperature, while oxide ion conduction is favored at higher temperature. Experimental results on $BaCe_{0.95}Y_{0.05}O_{3-\delta}$ in our laboratory also showed this trend [9]. Recently, substitution of Ba with other

*Corresponding author. Tel.: +1 630 2524250; fax: +1 630 2523604; e-mail: u_balachandran@qmgate.anl.gov

0167-2738/98/$19.00
PII: S0167-2738(98)00148-9

elements having different ionic radii was used to tailor proton and oxide ion conduction [10]. By substituting Ca for Ba, the lattice was much distorted from its pseudo-cubic structure; and as a result, the oxide ion conduction was greatly reduced while the proton conduction was only slightly affected [10].

According to Knight [11] and Bonanos et al. [12], the more distorted orthorhombic structure of $SrCeO_3$ inhibits oxide ion conduction but has little influence on proton conduction. Consequently, protonic conduction may be more highly favored in $SrCeO_3$-based materials than in $BaCeO_3$-based materials; thus, in terms of hydrogen selectivity, the former materials may be more suitable for hydrogen separation.

In this study, impedance spectroscopy, open-cell voltage (OCV) measurements, and gas permeation measurements were used to determine the conductivities, transference numbers, and interfacial polarizations of $SrCe_{0.95}Y_{0.05}O_{3-\delta}$, in an effort to assess the potential of a material for application in hydrogen gas separation.

2. Experimental

2.1. Sample preparation

Powders of $SrCe_{0.95}Y_{0.05}O_{3-\delta}$ were prepared by solid-state reactions. $SrCO_3$ (Mallinckrodt), CeO_2 (Trona Chemicals), and Y_2O_3 (Trona Chemicals) in the desired stoichiometric ratio were ball milled for at least 24 h with isopropyl alcohol and then pan-dried and sieved. The mixture was first calcined for 12 h at 1000°C in air and then ground and recalcined in air for 10 h at 1200°C. The resulting powders, confirmed by X-ray diffraction to exhibit the orthorhombic perovskite structure, were then uniaxially pressed into 2.2 cm diameter pellets under a pressure of $\approx$200 MPa. The density of pellets sintered in air at 1500°C for 10 h (Fig. 1) was $>$90% of the theoretical value. Platinum paste (Heraeus CL11-5100) was screen-printed on polished surfaces of crack-free, 0.11 cm thick pellets, which were subsequently fired in air at 1200°C for 12 min to form porous electrodes (electrode area 0.49 cm^2) for electrochemical measurements.

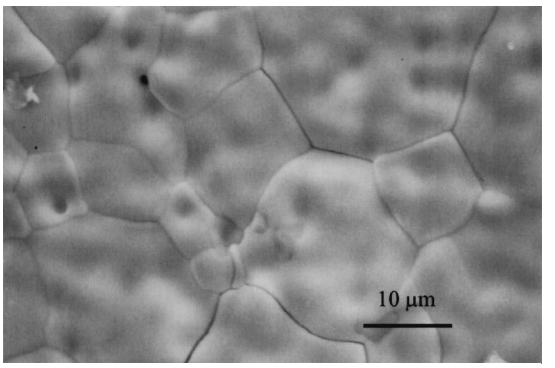

Fig. 1. SEM photomicrograph of as-sintered surface of $SrCe_{0.95}Y_{0.05}O_{3-\delta}$.

2.2. Impedance measurements

The sample to be tested was affixed to a test setup [9] with the aid of a glass sealant. The total conductivity was measured with an impedance analyzer (HP4192A LF) in the frequency range of 13 MHz–5 Hz under open-circuit conditions. Water vapor was introduced by bubbling desired gases through deionized water either at room temperature or at 40°C in an isothermal water bath (Polyscience, 7305). The partial vapor pressure of the water was monitored through an instant digital hygrometer (Fisher Scientific).

2.3. Ionic transference numbers

Transference numbers were determined by measuring either OCV or water vapor evolution. OCVs of fuel cells and concentration cells, measured by a high-impedance digital multimeter (HP 3446A), were used to estimate the ionic and electronic transference numbers. The ionic transference numbers so obtained may be underestimated in some cases because of interfacial polarization [13]. The evolution of water vapor by discharging an O_2/H_2 fuel cell was used to determine the ratio of proton and oxide ion transference numbers to the total ionic transference numbers. The gas inlets in the setup were positioned as close as possible to the test sample. Gas flow rates were adjusted to 50–100 $cm^3\,min^{-1}$. Water vapor concentration in both cathode and anode sides was measured with the

digital hydrometer under open-circuit and short-circuit conditions.

2.4. H_2 permeation

The hydrogen gas permeation rate was estimated from the measured short-circuit currents by applying Faraday's law. Also, the permeation rate under short-circuit conditions was predicted from the measured proton conductivities.

3. Results and discussion

3.1. Total conductivity

Total conductivities were determined from the impedance spectra of cells based on $SrCe_{0.95}Y_{0.05}O_{3-\delta}$ exposed to various atmospheres:

100% O_2, Pt|$SrCe_{0.95}Y_{0.05}O_{3-\delta}$|Pt,
4% H_2 + Ar (Cell 1)

4% H_2 + Ar, Pt|$SrCe_{0.95}Y_{0.05}O_{3-\delta}$|Pt,
0.488% H_2 + Ar (Cell 2)

O_2 + 2.64% H_2O, Pt|$SrCe_{0.95}Y_{0.05}O_{3-\delta}$|Pt,
7.79%O_2 + 2.64% H_2O + N_2 (Cell 3)

100% O_2, Pt|$SrCe_{0.95}Y_{0.05}O_{3-\delta}$|Pt,
8%O_2 + N_2 (Cell 4) .

Observed impedance spectra and calculated total conductivities in various atmospheres are shown in Fig. 2 and Fig. 3, respectively. Total conductivities, as determined in Cell 4 (dry O_2 concentration cell), were greater than those in Cell 2 (dry H_2 concentration cell). When compared with $BaCe_{0.95}Y_{0.05}O_{3-\delta}$ [9], the total conductivity of $SrCe_{0.95}Y_{0.05}O_{3-\delta}$ was lower in both oxygen and hydrogen. Surprisingly, the addition of water vapor into O_2 reduced the total conductivity in the temperature range studied. One plausible explanation was based on the consumption of electron holes to create protonic species when water vapor was added [3,14]. The conductivities in Cell 1 (O_2/H_2 fuel cell)

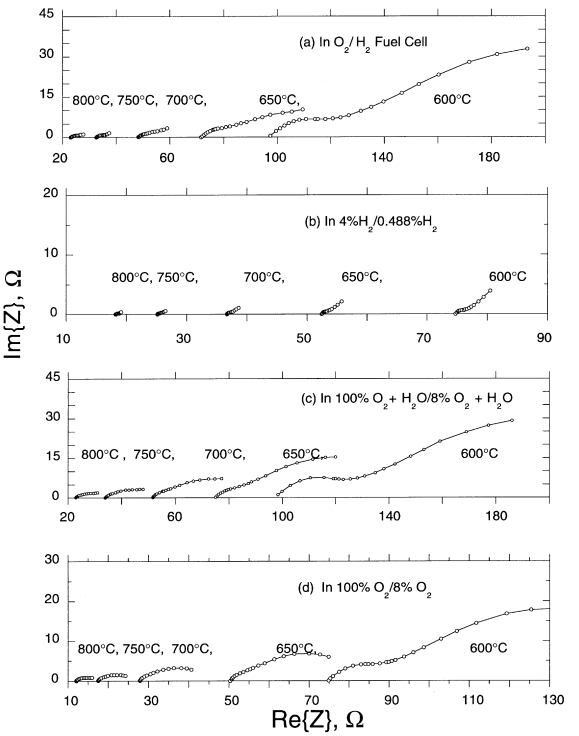

Fig. 2. Impedance spectra in various atmospheres: (a) Cell 1, (b) Cell 2, (c) Cell 3, and (d) Cell 4, all described in the text; electrolyte thickness, 0.11 cm; projected electrode area, 0.49 cm^2.

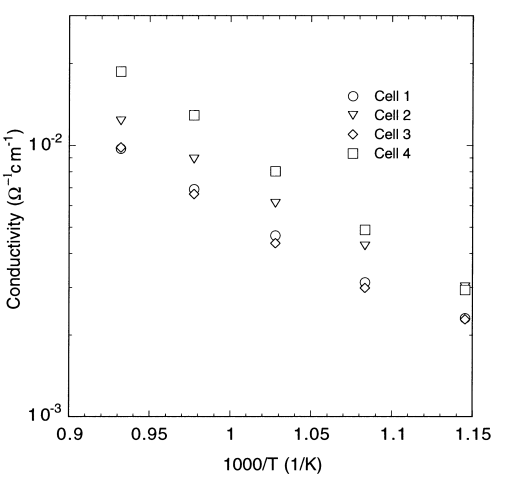

Fig. 3. Total conductivities determined from impedance spectra obtained in the various atmospheres shown in Fig. 2.

were lower than those in Cells 2 and 4 and were slightly higher than those in Cell 3 (wet oxygen concentration cell).

3.2. Ionic transference numbers

3.2.1. In O_2/H_2 fuel cell

Total ionic and electronic transference numbers were estimated from the OCV measurements of Cell 1. In this cell, we did not intentionally add water vapor to either side of the cell and the hydrogen concentration in the anode side was only 4%. The humidity detected in cathode side (oxygen side) using hygrometer varied from 200 to 500 vol ppm under open-circuit conditions at various temperatures. Such an amount of water vapor was believed to come from the diffusion of hydrogen either across the membrane itself or from the sealing area. A similar amount of water vapor was observed in the anode side (hydrogen side) because of oxygen diffusion. In terms of mixed ionic conduction, doped $SrCeO_3$ is more likely to be a proton conductor than an oxide ion conductor [11,12]. Thus, the Nernst potential E_N of the O_2/H_2 cell can be estimated from the hydrogen partial pressure in the anode side as well as from the oxygen partial pressure and water vapor pressure in the cathode side. Shown in Fig. 4 are the measured OCVs and the Nernst potentials that were calculated from the equation

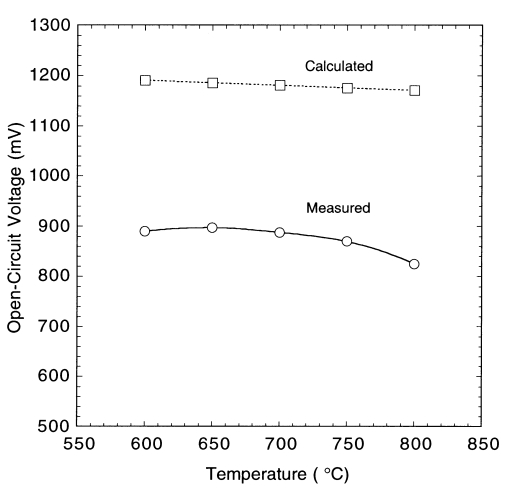

Fig. 4. Measured open-cell voltages and calculated Nernst potentials across the cell of with 100% O_2/4% H_2+Ar (Cell 1).

$$E_N = E^{\circ}(T) - \frac{RT}{2F}\ln\left(\frac{p_{H_2O}}{p_{H_2}p_{O_2}^{1/2}}\right) \quad (1)$$

by using a water vapor pressure of 50 Pa (≈500 vol ppm in concentration), where R is the universal gas constant, T is the absolute temperature, F is the Faraday constant, and $E^{\circ}(T)$ is the standard EMF calculated from

$$\Delta G^{\circ}(T) = -2E^{\circ}(T)F \quad (2)$$

and

$$\Delta G^{\circ}(T) = -247 + 0.056T\,, \quad (3)$$

where $\Delta G^{\circ}(T)$ is the standard formation energy (kJ mol^{-1}) of water vapor from reaction

$$H_2(g) + \frac{1}{2}O_2(g) \Leftrightarrow H_2O(g) \quad (4)$$

given in [15].

The total ionic transference numbers (oxide ion and proton) were then estimated to be ≈0.7 to 0.75 in the temperature range of 600–800°C from the measured OCVs and calculated Nernst potentials.

3.2.2. In hydrogen concentration cell

Total ionic transference numbers in a hydrogen atmosphere, which could be considered proton transference numbers, were estimated from the OCVs of Cell 2. Shown in Fig. 5 is the dependence of transference numbers on temperature. In the temperature range studied (600–800°C), the proton transference numbers changed from 0.90 to 0.86 while electronic transference numbers changed from 0.1 to 0.14. These results suggest that $SrCe_{0.95}Y_{0.05}O_{3-\delta}$ exhibits electronic conductivities that are inadequate for this material to be used as a membrane for hydrogen gas separation under ambipolar diffusion conditions [16].

3.2.3. In oxygen concentration cell

Total ionic transference numbers in an O_2/H_2O environment were estimated from OCV measurements on Cell 3. The proton and oxide ion transference numbers might be further separated from additional OCV measurements on Cell 5,

O_2 + 7.38% H_2O, Pt|$SrCe_{0.95}Y_{0.05}O_{3-\delta}$|Pt,
7.79%O_2 + 2.64%H_2O + N_2. (Cell 5) .

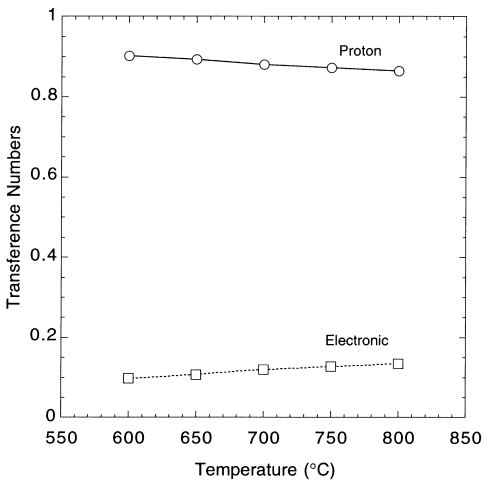

Fig. 5. Proton and electronic transference numbers determined from OCVs of the cell with 4% H_2/0.488% H_2 (Cell 2).

Ionic transference numbers t_{H^+} and $t_{O^{2-}}$ in an O_2/H_2O environment can be obtained by solving the OCV expressions for Cell 3 and Cell 5 [9],

$$V_{oc} = \frac{RT}{4F}\left[(t_{O^{2-}} + t_{H^+})\ln\left(\frac{p^{II}_{O_2}}{p^{I}_{O_2}}\right) - 2t_{H^+}\ln\left(\frac{p^{II}_{H_2O}}{p^{I}_{H_2O}}\right)\right]. \quad (5)$$

As shown in Fig. 6, the total ionic transference numbers decreased from 0.77 to 0.42 when temperature increased from 600 to 800°C. The oxide ion transference numbers did not change much, whereas proton transference numbers decreased from 0.45 to 0.17 when temperature increased from 600 to 800°C. The proton and oxide ion transference numbers were almost the same at ≈730°C, below which proton transference numbers were greater than oxide ion transference numbers.

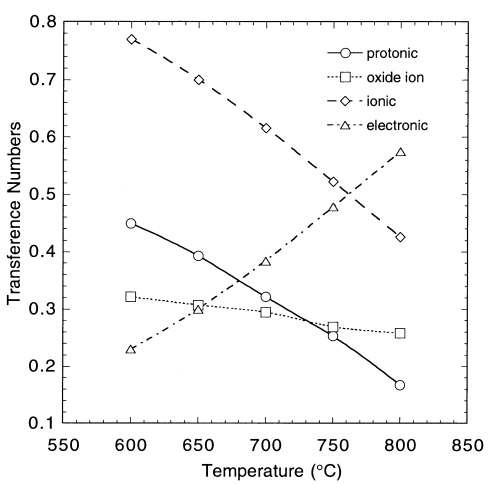

Fig. 6. Transference numbers determined from OCVs of Cells 3 and 5.

3.3. Determination of ratios of t_{H^+}/t_{ion} and $t_{O^{2-}}/t_{ion}$

The ratios of proton and oxide ion transference numbers to the total ionic transference numbers (t_{H^+}/t_{ion} and $t_{O^{2-}}/t_{ion}$) were further studied with Cell 1. The electrochemical process that occurs in the cell is schematically illustrated in Fig. 7a. When the two electrodes are set at equal potential, the current that passes through the electrolyte is approximately ionic while electronic current is negligible. Accordingly, the ratios of (t_{H^+}/t_{ion} and $t_{O^{2-}}/t_{ion}$) can be determined as follows:

$$\frac{t_{H^+}}{t_{ion}} = \frac{w_c}{w_t}, \quad (6a)$$

$$\frac{t_{O^{2-}}}{t_{ion}} = \frac{w_a}{w_t}, \quad (6b)$$

and

$$t_{ion} = t_{H^+} + t_{O^{2-}}, \quad (6c)$$

where w_c and w_a are the rates of water vapor evolution from the cathode and anode sides, respectively, and w_t is the total rate of water vapor evolution from both sides or the total rate of water evolution calculated from the short-circuit currents

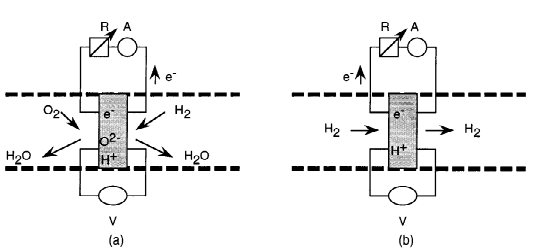

Fig. 7. Schematic illustration of electrochemical process that occurs in (a) Cell 1 and (b) Cell 2.

(when Faraday's law is applied). The rates of water vapor evolution due to the electrochemical process was calculated from the flow rates of carrier gas and humidity measured in both sides of the cell under open- and short-circuit conditions. The rate of water vapor evolution from the anode side (hydrogen side) was much slower than that from the cathode side (oxygen side), indicating that proton transport dominated the ionic transport. The total rate of water vapor evolution observed on both sides was in very good agreement with the rate calculated from short-circuit currents. As shown in Fig. 8, the ionic transference numbers are dominated by protons, even at 800°C. Unlike $BaCeO_3$-based materials [8,17], $SrCe_{0.95}Y_{0.05}O_{3-\delta}$ did not exhibit a conduction transition from proton to oxide ion as temperature increased from 600–800°C. In the temperature range studied, proton transference numbers were much higher than oxide ion transference numbers.

3.4. Polarization

The *I–V* characteristics of Cell 1 are shown in Fig. 9. The OCVs and the drop in IR calculated with the total impedance of the electrolyte are also presented. Thus, we can determine the overpotential, or polarization at the gas–solid interface, at each cell current. Based on an electrolyte with a thickness of 0.11 cm, the short-circuit current density of Cell 1 was ≈25 mA cm^{-2} at 750°C. The short-circuit current for Cell 2 was ≈0.8 mA cm^{-2} at 600°C and ≈2.8 mA cm^{-2} at 750°C. Fig. 10 shows the dependence of interfacial overpotentials on temperature and current density when Cells 1 and 2 were discharged as shown in Fig. 7. At a given discharging current in Cell 2, the overpotential decreased as temperature increased. At

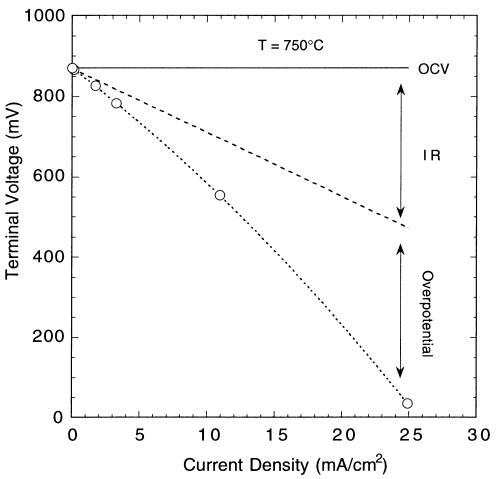

Fig. 9. *I–V* characteristics observed in Cell 1 at 750°C; electrolyte thickness, 0.11 cm; projected electrode area, 0.49 cm^2; gas flow rate, 50 $cm^3\ min^{-1}$.

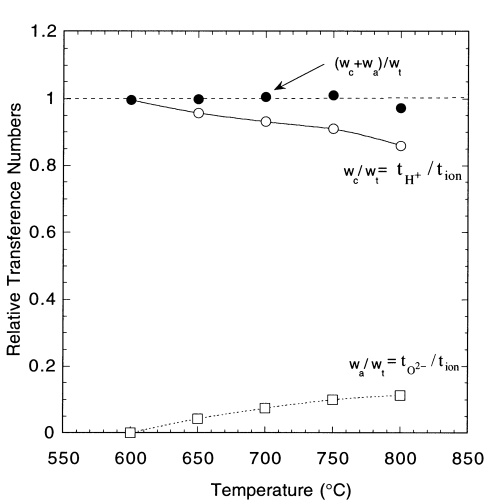

Fig. 8. Ratios of t_{H^+}/t_{ion} and $t_{O^{2-}}/t_{ion}$ determined from rates of water vapor evolution from cathode and anode sides of Cell 1.

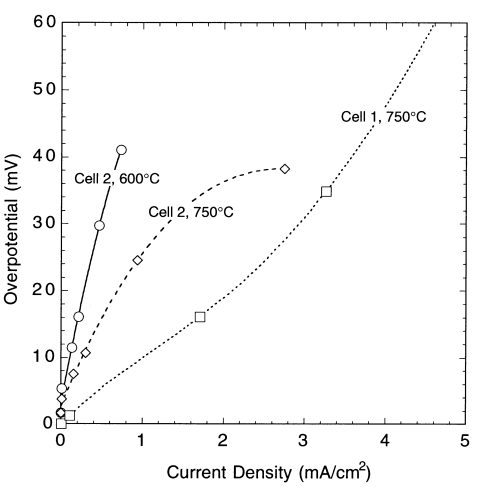

Fig. 10. Interfacial overpotentials in Cell 1 at 750°C and Cell 2 at 600 and 750°C; electrolyte thickness, 0.11 cm; projected electrode area, 0.49 cm^2; gas flow rate, 50 $cm^3\ min^{-1}$.

a given temperature and discharging current, the overpotential in Cell 1 (fuel cell) was lower than that in Cell 2 (hydrogen concentration cell).

3.5. H_2 permeation

The highest hydrogen permeation rate can be predicted from proton conductivity, assuming that the kinetics of the surface reaction are infinitely fast (or that no interfacial polarization occurs), as

$$N_{H_2} = (3.27 \times 10^{-4}) \times \frac{\sigma_{H^+} T}{L} \ln \left(\frac{p^{II}_{H_2}}{p^{I}_{H_2}} \right) \quad (7)$$

in terms of $cm^3\,(STP)\,cm^{-2}\,min^{-1}$.

The calculated permeation rate under the condition of Cell 2 (4%/0.488%) increased from $\approx$0.015 $cm^3\,(STP)\,cm^{-2}\,min^{-1}$ at 600°C to $\approx$0.072 $cm^3\,(STP)\,cm^{-2}\,min^{-1}$ at 800°C, with a 0.11 cm thick membrane. But the permeation rates from the short-circuit current measurements were only $\approx$0.006 $cm^3\,(STP)\,cm^{-2}\,min^{-1}$ at 600°C and $\approx$0.023 $cm^3\,(STP)\,cm^{-2}\,min^{-1}$ at 800°C (Fig. 11). The difference between the calculated rates from proton conductivity and short-circuit currents were probably due to the interfacial polarization, which consumed part of driving force, i.e., the difference in chemical potential across the bulk of the membrane, as schematically illustrated in Fig. 12. Thus, permeation rates can be significantly enhanced by improving the catalytic properties of the interface and further enhanced by reducing the thickness of the membrane [16,18].

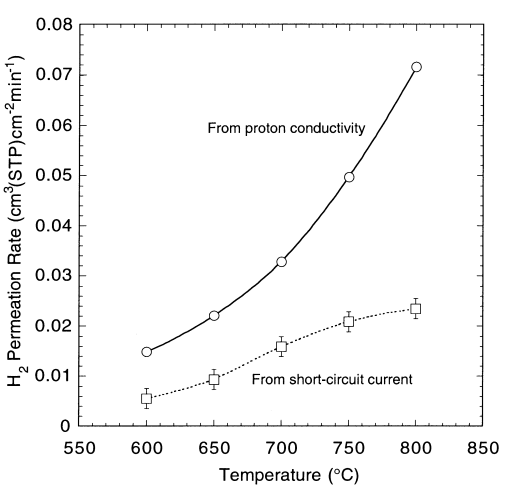

Fig. 11. Estimated hydrogen permeation rates under a gradient of 4% H_2/0.488% H_2 from proton conductivities and short-circuit currents.

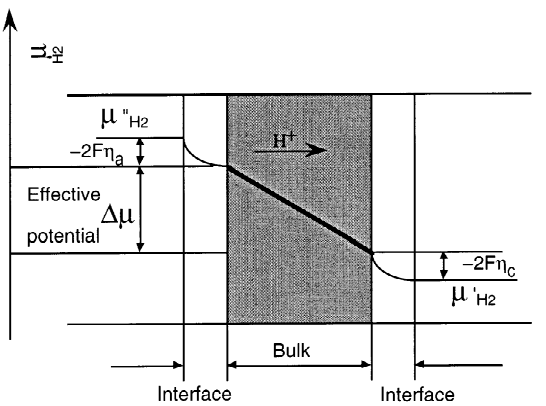

Fig. 12. Schematic illustration of overpotentials at interfaces and effective chemical potential across bulk of membrane.

4. Conclusions

Transport properties of $SrCe_{0.95}Y_{0.05}O_{3-\delta}$ were studied by impedance spectroscopy, and by measuring open-cell voltage and gas permeation measurements [15]. The ratios of the proton transference number and oxide ion transference number to the total ionic transference numbers were calculated from measured rates of water vapor evolution in an O_2/H_2 fuel cell. In the temperature range studied, the proton transference numbers were much greater than the oxide ion transference numbers. Permeation of hydrogen through a 0.11 cm thick membrane was demonstrated. Under a hydrogen gradient of 4%/0.488%, the hydrogen gas permeation rate was estimated from protonic conductivity measurements to be $\approx$0.072 $cm^3\,(STP)\,cm^{-2}\,min^{-1}$ at 800°C, whereas the permeation rate determined by measuring short-circuit currents was only $\approx$0.023 $cm^3\,(STP)\,cm^{-2}\,min^{-1}$. The difference between calculated and observed permeation rates was attributed to interfacial polarization. To maximize the hydrogen permeation rate through a

$SrCe_{0.95}Y_{0.05}O_{3-\delta}$ membrane, both conductivity and interfacial properties must be improved.

Acknowledgements

This work was supported by the U.S. Department of Energy, Federal Energy Technology Center, under Contract W-31-109-Eng-38.

References

[1] U. Balachandran, J.T. Dusek, S.M. Sweeney, R.B. Poeppel, R.L. Mieville, P.S. Maiya, M.S. Kleefisch, S. Pei, T.P. Kobylinski, C.A. Udovich, A.C. Bose, Am. Ceram. Soc. Bull. 74 (1995) 71.
[2] H.J.M. Bouwmeester, A.J. Burggraaf, in: A.J. Burggraaf, L. Cot (Eds.), Fundamentals of Inorganic Membrane Science and Technology, Elsevier Science, Amesterdam, 1996, p. 435.
[3] H. Iwahara, T. Esaka, H. Uchida, N. Maeda, Solid State Ionics 3–4 (1981) 359.
[4] D.A. Stevenson, N. Jiang, R.M. Buchanan, F.E.G. Henn, Solid State Ionics 62 (1993) 279.
[5] A.S. Nowick, Y. Du, Solid State Ionics 77 (1995) 173.
[6] H. Iwahara, T. Yajima, T. Hibino, H. Uchida, J. Electrochem. Soc. 140 (1993) 1687.
[7] N. Taniguchi, K. Hatoh, J. Niikura, T. Gamo, H. Iwahara, Solid State Ionics 53–56 (1992) 998.
[8] N. Bonanos, B. Ellis, M.N. Mahmood, Solid State Ionics 44 (1991) 305.
[9] J. Guan, S.E. Dorris, U. Balachandran, M. Liu, Solid State Ionics 100 (1997) 45.
[10] H. Iwahara, T. Mori, T. Hibino, Solid State Ionics 79 (1995) 177.
[11] K.S. Knight, Mater. Res. Bull. 30(3) (1995) 347.
[12] N. Bonanos, K.S. Knight, B. Ellis, Solid State Ionics 79 (1995) 161.
[13] M. Liu, H. Hu, J. Electrochem. Soc. 143 (1996) L109.
[14] D.A. Shores, R.A. Rapp, J. Electrochem. Soc. 119 (1972) 300.
[15] D.R. Lide, H.P.R. Frederikse, CRC Handbook of Chem. Phys. 77th Ed., CRC Press, 1996.
[16] M. Liu, in: T.A. Ramanarayanan, H.L. Tuller (Eds.), Proc. 1st International Symp. on Ionic and Mixed Conducting Ceramics, The Electrochemical Society, Pennington, NJ, 91-12, 1991, p. 191.
[17] H. Iwahara, T. Yajima, H. Uchida, Solid State Ionics 70–71 (1994) 267.
[18] M. Liu, in: T.A. Ramanarayanan, H.L. Tuller (Eds.), Proc. 1st International Symp. on Ionic and Mixed Conducting Ceramics, The Electrochemical Society, Pennington, NJ, 91-12, 1991, p. 95.